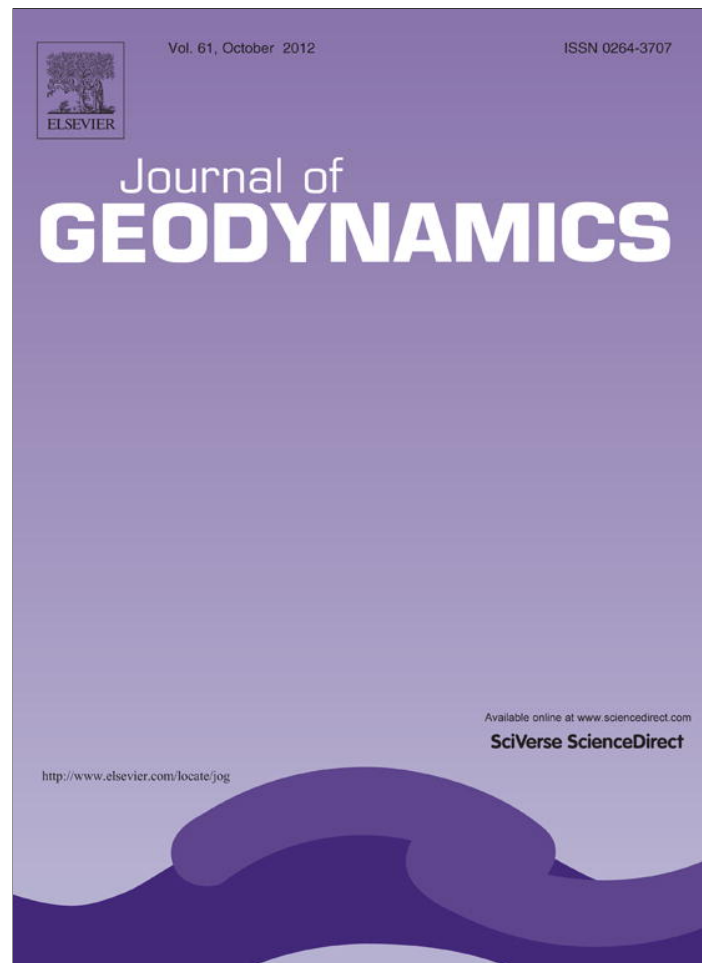


Provided for non-commercial research and education use.  
Not for reproduction, distribution or commercial use.



This article appeared in a journal published by Elsevier. The attached copy is furnished to the author for internal non-commercial research and education use, including for instruction at the authors institution and sharing with colleagues.

Other uses, including reproduction and distribution, or selling or licensing copies, or posting to personal, institutional or third party websites are prohibited.

In most cases authors are permitted to post their version of the article (e.g. in Word or Tex form) to their personal website or institutional repository. Authors requiring further information regarding Elsevier's archiving and manuscript policies are encouraged to visit:

<http://www.elsevier.com/copyright>



Contents lists available at SciVerse ScienceDirect

Journal of Geodynamics

journal homepage: <http://www.elsevier.com/locate/jog>

## Aftershock analysis of the 2005 November 27 (Mw 5.8) Qeshm Island earthquake (Zagros-Iran): Triggering of strike-slip faults at the basement

F. Yaminifard<sup>a,\*</sup>, M. Tatar<sup>a</sup>, K. Hessami<sup>a</sup>, A. Gholamzadeh<sup>b</sup>, E.A. Bergman<sup>c</sup>

<sup>a</sup> International Institute of Earthquake Engineering and Seismology (IIEES), Arghavan St., N. Dibaji, Farmanieh, Tehran 19537-14453, Islamic Republic of Iran

<sup>b</sup> Department of Physics, University of Hormozgan, Islamic Republic of Iran

<sup>c</sup> Department of Physics, University of Colorado, United States

### ARTICLE INFO

#### Article history:

Received 17 April 2011

Received in revised form 28 February 2012

Accepted 8 April 2012

Available online 16 April 2012

#### Keywords:

Aftershock  
Basement fault  
Qeshm Island  
Strike-slip  
Zagros

### ABSTRACT

From 2005 December 2 to 2006 February 26, a dense seismological network of 17 stations was installed in the epicentral region of the 2005 November 27 Qeshm sequence. The epicentral distribution of aftershocks, including an ENE–WSW trend of seismicity, is terminated on both sides by NW–SE alignments of events. The depth distribution of events (i.e., 8–20 km depth) is diffuse but in the eastern part of the aftershock zone reveals an alignment of seismicity dipping  $\sim 40^\circ$  toward the NW. Focal mechanisms of the aftershocks are strike-slip, different from that of the mainshock, which had a reverse mechanism. The scenario of a mainshock at shallow depth which is followed by a separated, deeper aftershock sequence implies different mechanisms of deformation in the sedimentary layer and the basement at the western edge of the Hormuz Strait. The epicentral distribution of aftershocks and their focal mechanisms suggest that shortening in the basement, due to convergence between Arabia and Eurasia, is accommodated in this region mainly by strike-slip motions.

© 2012 Elsevier Ltd. All rights reserved.

### 1. Introduction

An earthquake with magnitude Mw 5.8 occurred on Qeshm Island, on the western edge of the Strait of Hormuz in SE Zagros, on November 27, 2005. This earthquake destroyed 3 villages completely (Gavarzin, Zirang and Tonbha) and killed 10 persons. An interesting feature of this earthquake is the strike-slip mechanism of the strongest aftershock (Mw 5.4) that occurred  $\sim 6$  h after the mainshock, completely different from the pure reverse mechanism of the mainshock (Fig. 1).

Very little is known about the seismicity of this region. Historically, only one moderate event, in 1361, occurred in Qeshm Island but it is not well documented (Ambraseys and Melville, 1982). According to Engdahl et al. (2006) few well-located earthquakes near the island in recent decades. Therefore the information from the November 27 earthquake and its aftershocks may help to improve our knowledge about the seismotectonic framework of this seismically quiet part of the Zagros Mountains.

To study the aftershock sequence, we deployed a temporary network around the epicentral zone (Fig. 2), beginning 5 days after the mainshock and continuing for  $\sim 10$  weeks. The main questions that we wish to answer are, what is the geometry of the fault related to

the main-shock? What is the depth range of the aftershocks in this region of the Zagros? What is the reason for the existence of such different focal mechanisms for the mainshock and the largest aftershock? How is deformation distributed in the southeastern-most part of the Zagros? And, is high-resolution analysis using local data consistent with teleseismic and radar interferometry studies?

### 2. Geological setting and active faulting in the Zagros

The NW–SE trending Zagros Mountains extend for about 1700 km from NE Turkey to the Strait of Hormuz, where the north–south trending Zendan–Minab–Palami fault system (ZMP), separates the Zagros Mountains from the Makran accretionary prism. The northeastern edge of the Zagros Mountains is marked by the Main Zagros Reverse Fault (MZRF) which forms a steeply NE-dipping to sub-vertical reverse fault with a right-lateral component of movement (Stöcklin, 1974; Berberian, 1995). There is no clear surface boundary to the frontal edge of the Zagros deformation front, however, the southern edge of the Zagros front can be defined by the seismicity and topography (Jackson and McKenzie, 1984).

Deformation within the Zagros Mountains is due to the relative convergence between Arabia and Eurasia since the Middle-Late Cretaceous (Falcon, 1974; Stöcklin, 1974), however, the Zagros mountain belt formed during the main phase of the Zagros orogeny in Late Miocene to recent times (Stoneley, 1981; Hessami et al.,

\* Corresponding author. Tel.: +98 21 22831116 19; fax: +98 21 22289455.  
E-mail addresses: faryam@iiees.ac.ir, fyaminif@yahoo.fr (F. Yaminifard).

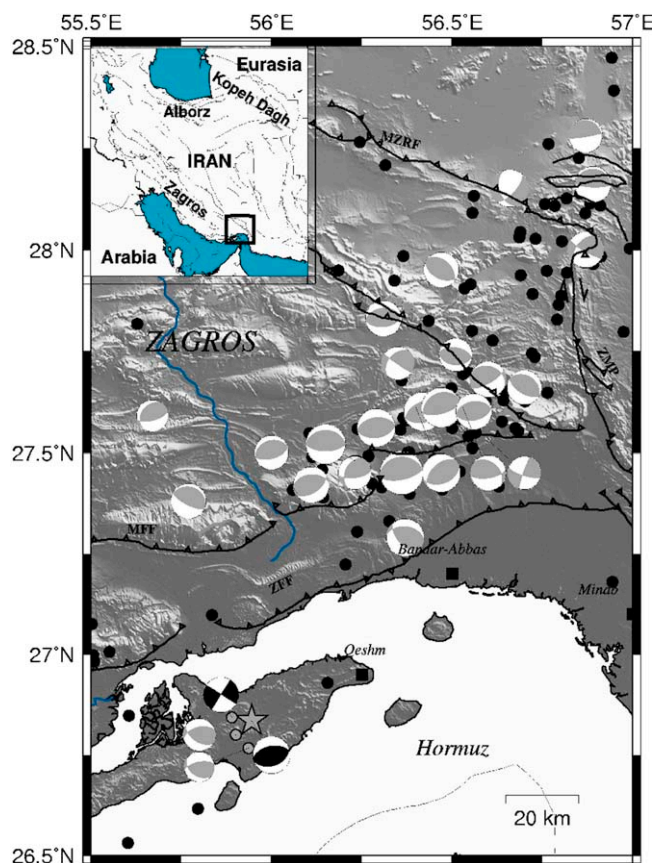


**Fig. 1.** Seismicity of the eastern end of the Zagros from 1964 to 2004 (Engdahl et al., 2006). Star is epicenter of the November 27 2005 10:22 UTC earthquake and gray circles are aftershocks. Focal mechanisms with gray color are from the Harvard University CMT catalog (<http://www.seismology.harvard.edu/CMTsearch.html>) and black ones are from teleseismic body-waveform modeling (Nissen et al., 2010).

2001). Current shortening at a rate of about 7 mm/y (Tatar et al., 2002; Vernant et al., 2004; Hessami et al., 2006) as well as active seismicity indicate that this deformation is still active.

Most focal mechanism solutions of earthquakes in the Zagros Mountains indicate the presence of active reverse faults in the basement (Tatar et al., 2004). The most recently determined focal depths (8–15 km) (Tatar et al., 2004) imply that moderate to large earthquakes occur in the uppermost part of the Arabia basement, which is decoupled from the overlying sedimentary cover along the Hormuz Salt Formation. These observations have led many workers

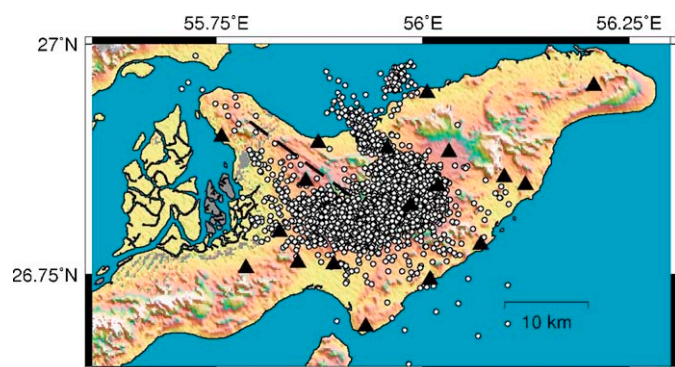


**Fig. 2.** Configuration of the seismic network installed in Qeshm Island from December 2, 2005 to February 26, 2006. Triangles are seismic stations. Gray circles show the epicentral distribution of all 2617 located aftershocks. Dashed line shows the Laft anticline axis.

**Table 1**

Crustal velocity structure of Qeshm-Island, based on 1-D inversion method of first-arriving P phases.

Top of the layer (km)	P velocity (km/s <sup>-1</sup> )
0	5.5
8	5.9
12	6.2

to suggest NE-dipping reverse faults in the basement (Jackson and Fitch, 1981; Jackson and Mckenzie, 1984; Ni and Barazangi, 1986; Berberian, 1995; Tatar et al., 2004).

Strike-slip faults in the basement beneath the sedimentary layer of the Zagros Mountains have also been inferred from seismological evidence and from the associated lateral offset of fold axes observed on geological maps and satellite images (Hessami et al., 2001; Talebian and Jackson, 2004). The presence of strike-slip faults in the Zagros basement suggests that some of the convergence between Arabia and Eurasia is accommodated by rotation of fault-bounded blocks about vertical axes and extension of the crust along the strike of the belt as well as by crustal shortening and thickening along thrust faults (Hessami et al., 2001).

### 3. Data analysis

From December 2, 2005 to February 26, 2006 a dense seismological network of 17 short-period seismographs was installed in the epicentral region of the November 27, 2005 Qeshm Island earthquake in order to infer the precise geometry of the aftershocks sequence in the fault region (Fig. 2). Recording was continuous at 100 samples per seconds. 2617 events recorded by at least three stations were extracted from the continuous data and located.

After initial processing, all events were located using a velocity model provided for the Zagros region (Hatzfeld et al., 2003) and the “Hypocenter” program (Lienert et al., 1986). To improve the velocity model, we selected a subset of 295 events recorded by at least 10 stations with an azimuthal gap less than 180°, an rms less than 0.2 s and uncertainties in epicenter and depth of less than 2 km. With these criteria the trade off between the velocity structure and the location of the events is small. Plotting  $T_{sj} - T_{si}$  (s arrival time to stations  $i$  and  $j$ , respectively for same event) versus  $T_{pj} - T_{pi}$  ( $p$  arrival time to stations  $i$  and  $j$ , respectively for same event) we compute a  $V_p/V_s$  ratio of  $1.8542 \pm 0.002$  from 2544 arrival times.

As we could find no detailed information on the velocity structure in the Qeshm Island area, we developed our own model. We first inverted the arrival times of the selected set of events for a 1-D velocity structure using the program VELEST (Kissling, 1988). Because the inversion result is strongly dependent on the starting velocity model, we explored 100 initial models randomly distributed (with differences as large as 0.5 km/s<sup>-1</sup> in each layer) around our starting model. We kept only the solutions for which the 1-D inversion converges well (e.g., rms decreases significantly to values less than 0.1 s). We started with a half-space velocity model composed of a stack of layers 2 km thick. This multilayered model is useful for locating major velocity discontinuities but we did not use it to describe the final velocity model because the number of unknowns is too large. The results of these experiments suggest that no more than 3 layers can be resolved. We computed the final velocity model by averaging all the inversions that converged (Table 1). The shear velocity for each layer was calculated from the  $V_p/V_s$  ratio 1.85. The corresponding average rms for the selected set of data is 0.12 s (0.16 s for the entire data set).

We calculated 183 focal mechanisms using a minimum of 8 P-wave polarities on the focal sphere (Appendix A). Considering the quality of the polarity reading and the azimuthal coverage on the focal sphere, we separated the solutions into two categories, A and

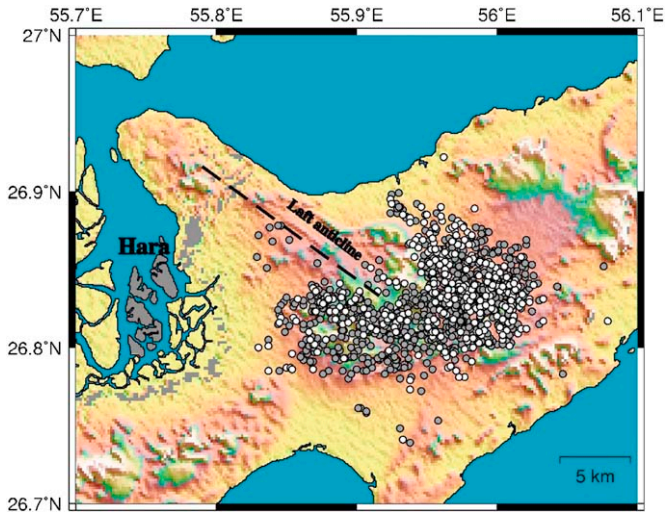


**Fig. 3.** Aftershock seismicity at two level of quality. Gray circles are 1222 events that meet the criteria: rms < 0.2 s, erz < 2 km, erh < 3 km, gap < 180°, and recorded by more than 5 stations. White circles are 326 events meeting stricter criteria: rms < 0.2 s, erz < 2 km, erh < 2 km, gap < 180°, and recorded by more than 8 stations.

B, in which the two nodal planes are constrained within 5° and 10°, respectively.

#### 4. Aftershock seismicity

Among all 2617 events that we located (Fig. 2), we kept 1222 aftershocks with horizontal and vertical errors less than 2 km and 3 km respectively, rms < 0.2 s, and having at least five *P* and two *S* readings. The distribution of these higher quality locations (gray circles in Fig. 3) shows a ~ENE–WSW trend almost parallel to the main trend of Qeshm Island. Alignments of events trending NW–SE are observed at both ends of this trend. A separate cluster of aftershocks is located to the northeast. However, a diffuse arcuate pattern reflecting the topography is roughly observable from the entire data set.

In order to ensure our interpretation of the aftershock seismicity and of the related active fault, we consider 326 events fulfilling the more stringent quality criteria: ERZ and ERH < 2 km, gap < 180°, RMS < 0.2 s, and recorded by minimum 8 stations (white circles in Fig. 3). This image again confirms the ENE–WSW trend of seismicity in addition to the NW–SE alignments of aftershocks located at the eastern edge, almost perpendicular to the main trend.

In order to reduce scatter in the locations due to local heterogeneity of the velocity structure and to refine our interpretation, we relocated the aftershocks as a cluster using the Double Difference method HypoDD (Waldhauser and Ellsworth, 2000). We chose to have pairs with a minimum of 10 links (travel times to station) and distance between events (belonging to the same pair) less than 8 km. The distribution of events relocated by Double Difference is very close to our single-event locations and confirms the main ~ENE–WSW trend of seismicity, in addition to the narrow NW–SE alignments of events at the eastern and western edges of the main trend (Fig. 4). No significant difference is observed between the HYPCENTER locations and the Double Difference relocations.

Calibrated relocation of the mainshock and largest aftershocks of the Qeshm sequence with the Hypocentroidal Decomposition method for multiple event relocation (Walker et al., 2011) indicates that the November 27, 2005 16:30 UTC aftershock (Mw 5.4) occurred 5–6 km northwest of the mainshock (Fig. 4, Table 2). The mainshock is located in the middle of the aftershock zone, with a location accuracy of about 2 km.

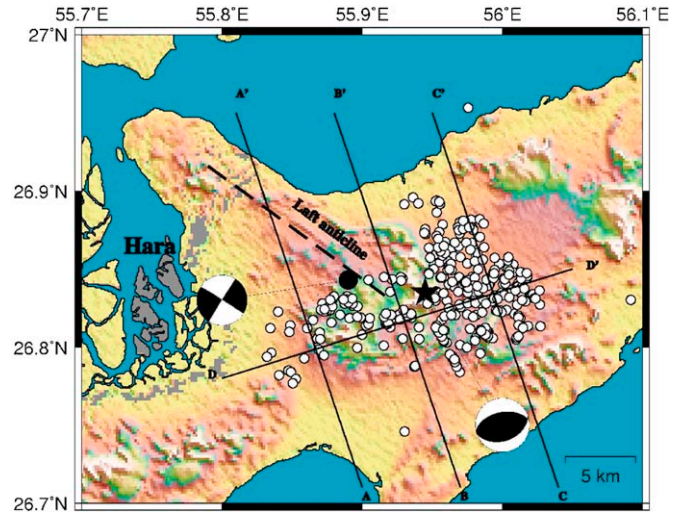


**Fig. 4.** Seismicity map of 326 selected events (rms < 0.2 s, erz < 2 km, erh < 2 km, gap < 180, recorded by more than 8 stations), relocated using the Double Difference method (Waldhauser and Ellsworth 2000). The star is the epicenter of the November 27, 2005 10:22 UTC mainshock and the gray circle is the largest aftershock, both relocated by a separate calibrated location analysis using local, regional, and tele-seismic data. Focal mechanisms are from Nissen et al. (2010). The locations of depth sections shown in Fig. 6 are indicated here.

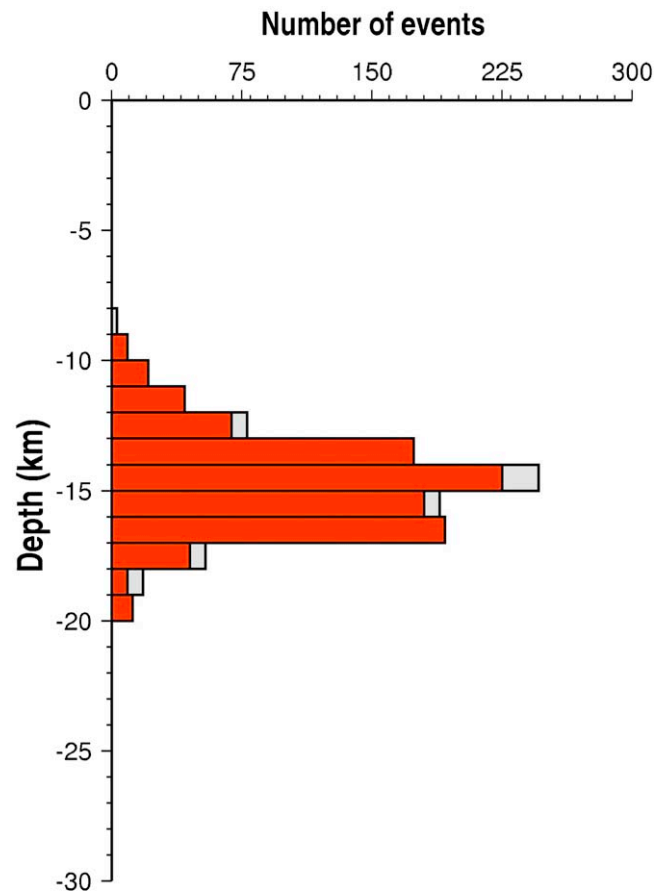


**Fig. 5.** Depth distribution of the 326 highest-quality aftershock locations, meeting the criteria: rms < 0.2 s, erz < 2 km, erh < 2 km, gap < 180°, and recorded by more than 8 stations. Red is for location by the multiple event code HYPODD and the gray is for single-event HYPCENTER locations. There is no seismic activity shallower than 8 km.

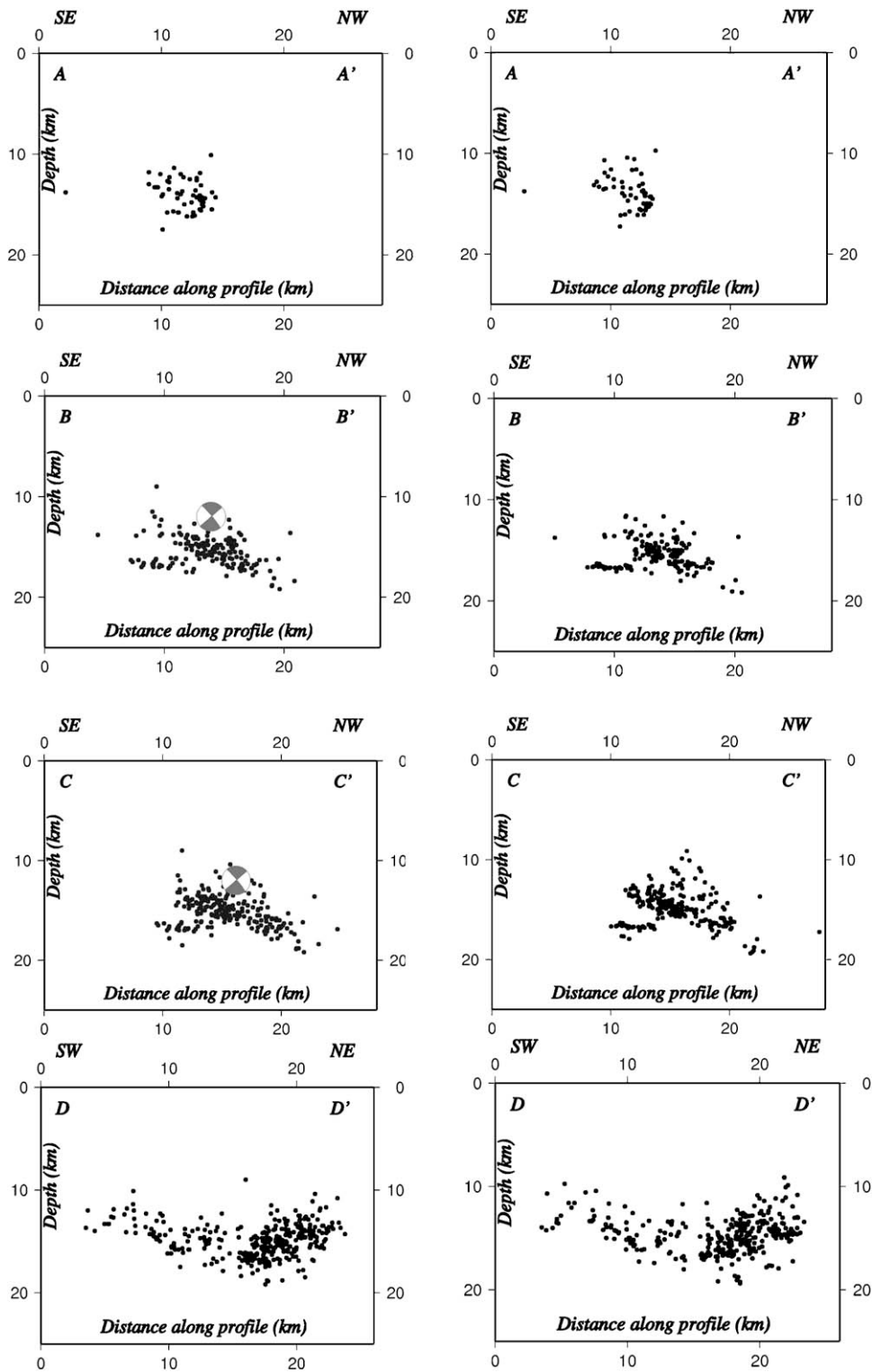


**Fig. 6.** Depth sections AA', BB' and CC' are perpendicular to the azimuth of mainshock nodal planes and the overall trend of aftershock seismicity. Section DD' is parallel to the dominant seismicity trend (Fig. 4 for depth section locations). The sections are 10 km wide. On the left are single-event locations by HYPOCENTER. On the right are relocations from the Double Difference method (Waldhauser and Ellsworth, 2000). An alignment of seismicity dipping at  $\sim 40^\circ$  toward the NW can be observed on BB' and CC' sections. The focal mechanism for mainshock is also shown (Table 2).

A histogram of the depth of the relocated aftershocks shows that the seismicity is located at depths between 8 and 20 km but the majority are located between 13 and 17 km, very similar to the depth range of microseismicity in the Central and High Zagros (Tatar et al., 2004; Yaminifard et al., 2006), and likely beneath the sedimentary layer (Fig. 5).

To investigate further the distribution of aftershocks with depth, we formed three SE–NW sections (see Fig. 4 for locations of cross sections on the map), each with a width of 10 km, striking perpendicular to the main trend of seismicity and the azimuth of the nodal planes of the mainshock (Fig. 4, Table 2 we also formed one depth section on a SW–NE axis, parallel to the main trend

**Table 2**  
Parameters of the focal mechanisms for the November 27, 2005 mainshock and the 3 largest aftershocks (Nissen et al., 2010): Lat, Lon and Depth are the coordinates of the earthquakes based on a calibrated multiple event analysis using local regional and teleseismic data. Mag is the moment magnitude, Az, R, Di are Azimuth, rake and dip of nodal plane 1. Saaz, XI and Avh are Semi-axis azimuth, Semi-axis length in km and geometric area, in km<sup>2</sup>, of 90% confidence ellipse.

No	Date	Time	Lat	Lon	Depth	Mag	Di1	Az1	R1	Saaz1	XI1	Saaz2	XI2	Avh
1	20051127	10:22:18.63	26.835	55.945	12	5.8	50	71	95	64	1.1	154	1.3	5
2	20051127	11:13:10.05	26.800	55.901	14	5.0	49	124	52	69	1.2	159	1.4	5
3	20051127	16:30:36.11	26.843	55.890	9	5.4	89	302	358	65	1.2	155	1.4	5
4	20051130	15:19:55.97	26.767	55.936	15	4.7	62	127	62	284	1.4	14	1.5	7

of seismicity. We formed the images from the 326 best-located events (ERZ and ERH < 2 km, gap < 180°, RMS < 0.2 s, recorded by minimum 8 stations).

The western cross section, AA', (Fig. 6) shows a diffuse pattern of seismicity between 10 and 17 km. The distribution of focal depths on the middle cross section, BB', reveals a NW-dipping alignment of seismicity. This dipping pattern is also evident from the relocated aftershocks using the Double Difference method. A NW-dipping alignment of aftershocks can also be distinguished on section CC', in the eastern portion of the aftershock seismicity. Continuation of this pattern to the surface projects beyond Qeshm Island, in the Persian Gulf.

Section DD' (Fig. 6), located parallel to the trend of seismicity, shows that the deepest aftershocks occur in the central part of the epicentral region.

**5. Focal mechanisms**

Focal mechanisms of 183 selected aftershocks were computed using first motion data (Fig. 7, Appendix A). We selected the events that have an azimuthal open azimuth < 180° and at least eight polarity observations. A dominant component of strike-slip motion is recognizable in most of 183 computed focal mechanisms. We observe few aftershocks with focal mechanisms similar to that of the mainshock. The few examples with a significant component of reverse faulting are found in the eastern part of the epicentral region (e.g., no. 54).

Toward the central part of the main ENE–WSW alignment, we observe strike-slip focal mechanisms with P axes oriented NW (Figs. 8 and 9), consistent with right-lateral motion on faults that are subparallel to the seismicity pattern. However, we also observe some focal mechanisms (e.g., nos. 41 and 108) along the same trend that would be consistent with left-lateral motion along NW–SE-trending faults.

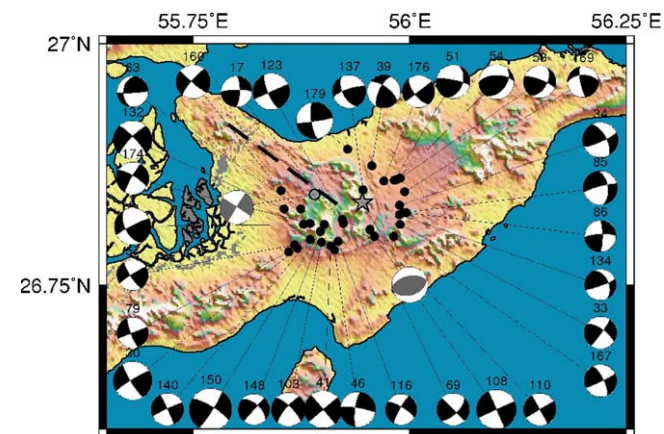


**Fig. 7.** Focal mechanisms for aftershocks,  $M_l \geq 3$ , indicating dominantly strike-slip mechanisms. Shaded quadrants are the compressional areas. Gray focal mechanisms are for mainshock and the largest aftershock (Table 2).

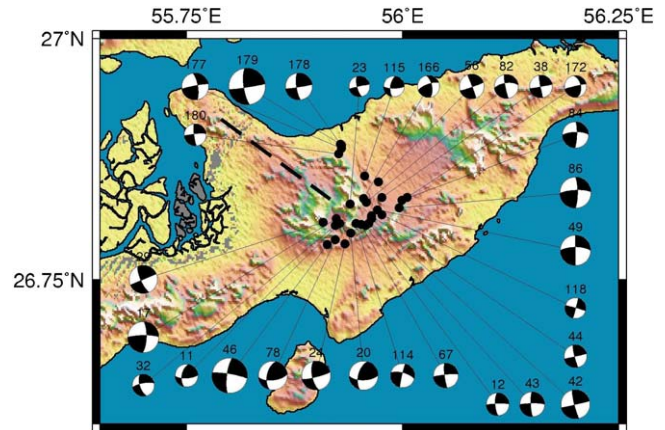


**Fig. 8.** Focal mechanisms for aftershocks,  $M_l \geq 2$ , with P axes in the NW direction, mostly located near the southern end of Laft anticline, in the middle of the aftershock zone. Shaded quadrants are the compressional areas.

At the western end or the epicentral region the majority of focal mechanisms indicate right-lateral strike-slip motion on NW–SE planes, similar to the mechanism of the largest aftershock at 16:30 UTC on November 27, 2005. The azimuths of P axes obtained from focal mechanisms are dominantly oriented to the NE at both ends of the main ENE–WSW alignment of seismicity (Fig. 9).

In general the aftershock mechanisms are different from that of the mainshock, are dominantly strike-slip, and they show systematic variations across the epicentral region, implying triggering of strike-slip movements and, combined with their depth distribution, with complex interactions in the basement.

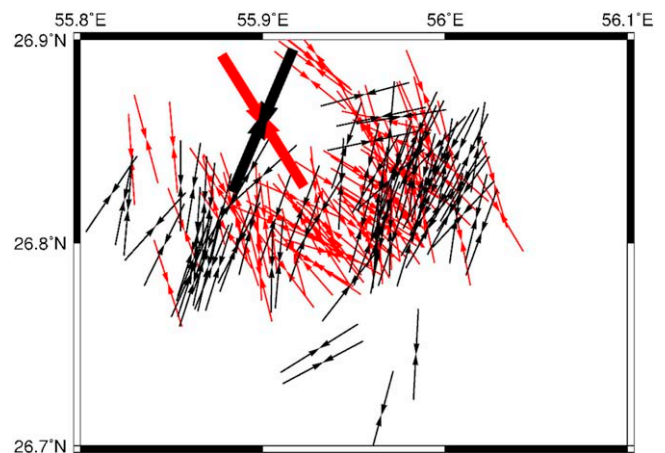


**Fig. 9.** Spatial distribution of P axis azimuths from all focal mechanisms, revealing two groups of focal mechanisms: those with P axes oriented NW and mostly located in the middle of the aftershock zone (red) and those with P axes oriented NE, mostly located at the ends of aftershock zone (black). Thick arrows illustrate the average of the azimuths for each group, N23E and N32W. (For interpretation of the references to color in this figure legend, the reader is referred to the web version of the article.)

## 6. Discussions

Previous research has emphasized the role of transverse strike-slip faults in the evolution of the Zagros basement (Talebian and Jackson, 2004). Focal mechanism solutions of the earthquakes along the transverse faults within the Zagros region are interpreted as steeply dipping strike-slip faults with minor components of dip-slip movement. Most of these solutions involve right-lateral movement on nodal planes parallel to NNW-trending faults (i.e., the Kazerun, Karebas and Sarvestan faults). The results of our investigation of the aftershocks of the 2005 Qeshm Island event reveal the importance of strike-slip faults in the basement of the southeastern-most Zagros.

The epicentral distribution of aftershocks, a broad arcuate shape, indicates one major alignment oriented ENE–WSW and two minor alignments in the NW–SE direction, bounding both ends of the main alignment. Cross sections perpendicular to the main trend of aftershocks show a pattern of seismicity dipping at  $\sim 40^\circ$  to the northwest. However, the focal mechanisms of aftershocks are dominantly strike-slip in character, distinctly different from the mainshock. Waveform modeling for the mainshock indicates a reverse fault mechanism with nodal planes dipping  $\sim 50^\circ$  N or  $40^\circ$  SSE, and a centroid depth of 9 km (Nissen et al., 2010). However, elastic dislocation modeling using Envisat Advanced Synthetic Aperture Radar (ASAR) data is consistent with slip on either a  $42^\circ$  north-dipping plane or a  $39^\circ$  NNE-dipping plane or a  $36^\circ$  SSE-dipping fault. The center of the fault plane in each model is located at 5.7–5.8 km. This implies that rupture was concentrated within the lower part of the sedimentary cover but it is not clear whether the bottom of the rupture zone extended into the uppermost crystalline basement (Nissen et al., 2010). However, this study indicates that the majority of aftershocks are located at depths of about 11–18 km, beneath the sedimentary layer. Our observation that the aftershock patterns displays a dip of  $40^\circ$  NW along the eastern part of the aftershock zone is consistent with the  $42^\circ$  N-dipping fault deduced from dislocation modeling. However, the more prevalent pattern of aftershocks dipping toward the northwest is more consistent with a NW-dipping fault (see BB' and CC' sections in Fig. 6). Our observations strongly support a model of vertical separation between the relatively shallow mainshock rupture and deeper microseismicity along the Hormuz salt formation, as suggested by Nissen et al., 2010. This would suggest that pre-existing basement faults have been triggered due to the large stress release during the November 27, 2005 mainshock.

The NW–SE alignment of seismicity at the west-southwestern end of the zone of aftershocks, where the shallower aftershocks are located, could be related to right-lateral strike-slip motion along the same trend. The location of the November 27, 2005 16:30 UTC aftershock (Mw 5.4) from Hypocentroidal Decomposition (Table 2), with an uncertainty less than 2 km, and the similarity of its mechanism to the focal mechanisms we determined using first motions of local earthquakes (Fig. 7), suggest right-lateral slip along a NW-oriented fault located near the axis of the Laft anticline, west of the mainshock epicenter.

As shown on the Geological Map of the Qeshm Area (Haghipour and Aghanabati, 2005) the main trend of the anticline axes of Qeshm Island are similar to the overall structural trend of the Zagros on the adjacent mainland (i.e., NE–SW). However, the axis of the Laft anticline, forming a complex structure in the central part of the island, trends NW–SE and therefore crosses the main structural trend of Qeshm Island. The most plausible explanation for this discrepancy is that the Laft anticline has been formed in its present form as a result of buckling associated with a basement strike-slip fault. It is believed that shear along a basement strike-slip fault induces compression in the cover rocks which

may produce folds sub-parallel with the causative basement fault (e.g., Price and Cosgrove, 1990). Therefore, we infer a NW-trending blind right-lateral strike-slip fault west of the Laft anticline axis that crosses the general structural trend of Qeshm Island. At the surface, the Gavazrin basement fault appears as several minor right-lateral strike-slip faults that run sub-parallel with the axis of the Laft anticline as it is shown on the Geological Map of the Qeshm Area (Haghipour and Aghanabati, 2005). Haghipour and Aghanabati (1996) attributed the negative Bouguer gravity anomaly observed near the Mangrove (Hara) forest to the Hormuz Salt dome at depth. However, we can attribute the rise of this dome to reactivation of the Gavazrin basement fault, which tears the overlying sediments and create extensional jogs, through which the salt extrudes. Our seismological observations support the existence of the Gavazrin right-lateral basement fault and indicate that it took part in the extended aftershock activity following the 2005 Qeshm mainshock.

There is also another NW-oriented trend of the aftershocks, at the northeast end of the zone of aftershocks east of the Laft anticline, that is consistent with right-lateral strike-slip motion along this trend (Fig. 2). Such a system of right-lateral strike-slip faults can accommodate N–S shortening by anticlockwise rotation about a vertical axis (Jackson and McKenzie, 1984).

Focal mechanisms along the main ENE–WSW trend of aftershocks show complex features and are consistent with both left- and right-lateral strike-slip motion (Figs. 7 and 8). Vectors of the P-axes for the focal mechanisms shows two dominant directions,  $N23^\circ E$  and  $N32^\circ W$  (Fig. 9) which are consistent with the overall relative motion of the Arabian plate toward central Iran, i.e.,  $\sim N10^\circ E$ , and the azimuth of the P axis of the mainshock focal mechanism, respectively (Vernant et al., 2004; Nissen et al., 2007, 2010). Similar differences are observed between the principal horizontal axes of geodetic observations, which show compressive strain toward the northeast, and seismic strain in the northwest compressional direction (Bayer et al., 2006).

The agreement between the deeper mechanisms and the convergent motion, suggests that the deformation of the upper crystalline crust, accommodated by strike-slip fault systems, is consistent with the overall motion of Arabia toward central Iran. The difference between that vector and the orientation of the P-axis of the mainshock within the sedimentary layer implies that the sedimentary cover does not accommodate shortening in the same way. Slip partitioning between strike-slip and thrust motions because of oblique convergence has been observed to the east of the Hormuz Strait, but with strike-slip deformation at shallow depths and pure thrust faulting at greater depths (Yaminifard et al., 2007).

## 7. Conclusions

A P velocity model for the Qeshm Island study area based on 1-D inversion of first arrival times consists of 2 layers over a half-space: an 8 km thick sedimentary layer (5.5 km/s) above a 4 km crystalline crustal layer (5.9 km/s), above a halfspace ( $V_p$  6.2 km/s). We calculated a high  $V_p/V_s$  ratio, 1.85, from the data set, suggesting low velocity S wave propagation in the upper crust beneath Qeshm Island that could be caused by fluids beneath Laft anticline, source of the Gavazrin gas field.

The pattern of aftershocks extends in a broad arcuate pattern oriented ENE–WSW, roughly parallel to the nodal planes of the reverse faulting focal mechanism of the mainshock. The majority of aftershocks of the November 27, 2005 Qeshm mainshock are located between 11 and 18 km depth with a tendency to deepen toward the NW. Therefore aftershocks have occurred mainly in the upper part of the crystalline crust even though the mainshock

appears to have ruptured mainly in the sedimentary cover. The Hormuz salt layer along the boundary of the sedimentary and crystalline basement likely plays a role in this partitioning.

The pattern of aftershock seismicity and the focal mechanisms calculated for many of them reveal the existence of a complex strike-slip fault system beneath the sedimentary layer. Our results are consistent with a model in which this strike-slip fault system in the basement was activated by stresses associated with the reverse mainshock rupture in the sedimentary layer. They suggest that different mechanisms of shortening are preferred between the upper crystalline basement and the sedimentary cover in the western Hormuz Strait. We propose that the aftershocks are mostly the result of accommodation of the convergence between the Arabian and Eurasian plates, by anti-clockwise rotation of fault-bounded blocks in the basement.

## Acknowledgements

We thank the IIEES team for support, administrative and field work assistance in very hard conditions. This work would not have been possible without the help of the people of Qeshm Island. We thank Mr. Mohammadian and Mr. Tahmasebi from the Qeshm Development Organization for their kind hospitality on Qeshm Island. Comments by anonymous reviewers helped improve both the presentation and interpretations of this paper.

## Appendix A.

Parameters of the aftershock focal mechanisms determined by phase polarities: Lat, Lon are the coordinates of the earthquake. Mag is the magnitude, Az, R, de are Azimuth, rake and dip of nodal plane 1. AzP, deP, AzT, deT are azimuth and dip of *P*-axis and *T*-axis. A and B are quality factor.

No	Date	Time	Lat	Lon	Depth	Mag	de1	Az1	R1	AzP	deP	AzT	deT	Q
1	20051206	302	26.838	55.98	16.3	2.8	83.59	42.07	-7.69	357.42	9.96	87	1	A
2	20051206	1201	26.812	55.877	14.7	3.5	86.09	243.84	33.8	12.59	20.14	112	26	A
3	20051206	1519	26.848	56.002	11.6	2.9	52.24	36.29	26.57	346.33	10.55	246	43	B
4	20051207	6	26.808	55.905	17.5	2.4	64.34	221.19	16.1	174.44	7.44	80	29	B
5	20051207	127	26.829	55.943	15.8	1.3	80	227.63	0	183.06	7.05	92	7	A
6	20051207	319	26.819	55.882	14.5	1.9	90	77	0	32	0	122	0	A
7	20051207	457	26.832	55.979	15.4	2.1	73.33	188.77	25.31	318.68	4.98	51	30	A
8	20051207	515	26.81	55.913	15.4	1.9	69	162	0	118.97	14.68	25	15	B
9	20051207	538	26.824	55.88	14.4	2.4	80.61	14.72	-3.45	330.34	9.05	239	4	B
10	20051207	1357	26.788	55.905	14.1	2.2	90	227.4	18	0.96	12.62	93	13	B
11	20051207	1416	26.808	55.927	15.5	2.2	56.97	191.34	23.97	142.11	8.31	45.37	39	A
12	20051207	1650	26.806	55.957	14.3	2.2	72.91	176.58	-5.73	133.62	15.98	41.3	8	B
13	20051207	1912	26.806	55.938	15.7	1.7	74.81	172.4	-13.2	129.49	19.92	38.87	2	A
14	20051207	2005	26.829	56.027	14.8	2	43.96	30.77	22.18	344.56	18.89	235.29	44	B
15	20051207	2129	26.805	56.02	14.9	1.5	64.34	67.02	16.1	20.27	7.44	286.14	29	B
16	20051207	2133	26.715	55.965	10	2.1	52.24	44.89	-26.6	14.87	43.08	274.85	11	B
17	20051207	2254	26.813	55.923	15.5	3	72.77	2.4	10.31	316.7	5.08	224.92	20	A
18	20051207	2307	26.815	56.03	15.3	1.4	60.5	21.08	28.34	329.64	3.21	236.96	39	B
19	20051207	2345	26.856	55.963	16.8	1.5	82.56	209.15	-13.1	164.5	14.48	255.49	3	B
20	20051208	1825	26.798	55.94	13.5	2.8	60.18	195.12	31.07	142.42	2.01	50.62	41	A
21	20051208	1833	26.795	55.944	15.4	1.8	70.79	172.11	29.84	300.17	5.72	34.1	34	A
22	20051208	2241	26.806	55.88	14.8	2.5	68	189	0	146.16	15.36	51.84	15	B
23	20051209	1244	26.828	55.939	15.5	2	72.07	165.99	-1.62	122.66	13.69	29.83	11	A
24	20051209	1535	26.787	55.933	15.6	2.8	67.84	169.14	9.47	124.09	9.14	30.36	21	A
25	20051209	1540	26.79	55.928	14	1.8	61.69	169.59	19.67	121.74	7.23	27.02	33	A
26	20051210	202	26.806	55.857	13.3	2.4	75.52	202.83	-3.97	159.2	12.95	67.48	7	B
27	20051210	1836	26.78	55.862	14.5	2.6	90	243.33	10	17.89	7.05	108.77	7	A
28	20051210	2254	26.811	55.964	16.5	1.3	87	49.91	5.2	184.7	1.55	274.86	5	B
29	20051211	148	26.809	55.908	15.5	2.7	75	156.67	0	112.66	10.55	20.67	10	B
30	20051211	242	26.788	55.87	13.1	3.7	84.43	238.66	8.32	13.09	1.9	103.42	9	A
31	20051211	300	26.795	55.861	15	2.1	90	243.33	10	17.89	7.05	108.77	7	A
32	20051211	321	26.806	55.922	14.5	2.1	64.34	162.71	-16.1	123.59	28.88	29.46	7	A
33	20051211	1328	26.812	55.989	14.1	3.1	84.68	35.91	20.34	168.28	10.32	261.69	18	A
34	20051211	1629	26.832	55.988	15.7	3.4	80.15	65.84	28.48	195.32	12.2	291.63	26	B
35	20051211	1910	26.833	55.993	13.9	1.7	81.35	62.05	5.04	16.88	2.58	286.45	9	B
36	20051213	53	26.785	55.861	13.5	2.3	90	243.33	10	17.89	7.05	108.77	7	A
37	20051213	507	26.831	55.968	13.4	2.4	50	21.09	0	343.63	27.03	238.54	27	B
38	20051213	520	26.835	55.976	15.5	2.2	87.2	169.69	1.08	124.7	1.22	34.64	2	A
39	20051214	504	26.873	55.956	14.8	3.2	65.63	306.43	25.94	255.92	0.57	165.52	34	B
40	20051214	516	26.862	55.965	13.9	2.4	79.53	301.72	-14.7	257.63	17.77	348.51	2	A
41	20051214	823	26.79	55.909	14.5	3.6	90	50	0	5	0	95	0	A
42	20051214	1353	26.813	55.964	16	2.8	84.13	166.73	1.25	121.81	3.26	31.52	5	A
43	20051214	1400	26.808	55.961	15.6	2.4	80.57	178.05	-7.46	133.82	11.91	43.52	1	B
44	20051214	1400	26.816	55.964	16.1	2.2	84.13	166.73	1.25	121.81	3.26	31.52	5	B
45	20051215	140	26.797	55.87	14.3	2.5	81.35	244.55	5.04	199.38	2.58	108.95	9	A
46	20051215	314	26.786	55.913	15.3	3.4	77.05	187.47	-7.63	143.84	14.48	52.84	3.84	B
47	20051215	1535	26.86	55.953	17.6	2.4	88.27	17.84	9.85	152.28	5.72	243.11	8.18	A
48	20051216	1432	26.78	55.848	13.6	2.2	82.65	207.95	9.51	342.18	1.45	72.49	11.91	B
49	20051216	1735	26.822	55.971	11.4	2.9	90	0	18	133.56	12.62	226.44	12.62	B
50	20051216	1909	26.812	55.907	13.4	2	81.02	243.65	-4.42	199.27	9.45	108.73	3.24	A
51	20051216	2125	26.858	55.982	12.3	3.3	43.86	22.69	15.04	340.35	22.5	230.33	39.57	B
52	20051217	154	26.811	55.799	11.6	1.5	61.61	194.59	23.12	145.36	5.28	51.59	35.49	A
53	20051217	544	26.86	55.989	12	3.1	52.84	30.63	16.01	345.56	15.76	243.89	35.63	B

No	Date	Time	Lat	Lon	Depth	Mag	de1	Az1	R1	AzP	deP	AzT	deT	Q
54	20051217	728	26.859	55.985	12.2	3.4	43.88	38.78	49.08	336.67	8.01	231.55	61.65	B
55	20051217	758	26.874	55.988	13.9	2.4	74.92	26.03	20.18	157.68	2.95	249.05	24.8	B
56	20051217	1012	26.851	55.972	13.4	2.4	86.79	339.89	-3.83	294.98	4.98	25.02	0.44	A
57	20051217	1427	26.791	55.867	14.1	3	84.75	237.98	11.91	11.94	4.62	102.93	12.12	A
58	20051217	1434	26.788	55.872	13.1	2.4	89.37	66.63	-5.97	21.51	4.66	111.82	3.77	A
59	20051218	21	26.8	55.971	14.6	2.6	87.26	62.64	-9.62	17.5	8.74	108.25	4.83	A
60	20051218	1220	26.841	55.828	12.6	2.4	64.34	215.48	-16.1	176.36	28.88	82.23	7.44	B
61	20051218	1707	26.825	55.929	16	2.4	75	218.33	0	174.33	10.55	82.34	10.55	B
62	20051219	251	26.815	55.932	15.8	2.1	90	77	0	32	0	122	0	B
63	20051219	440	26.828	55.874	14.3	3	41.03	186.05	11.69	146.48	26.06	33.27	38.87	B
64	20051219	1301	26.837	55.958	15.5	2.5	90	64.94	38	193.18	25.81	296.7	25.81	A
65	20051219	2351	26.808	55.841	12.1	1.9	72.99	270.3	17.19	222.8	0.41	132.62	24	B
66	20051220	1202	26.825	55.959	16.2	1.9	82.64	165.97	-20.8	120.62	19.85	213.94	9.11	A
67	20051221	738	26.807	55.952	15.7	2.4	82.36	173.73	-6.47	129.24	9.96	39.09	0.87	B
68	20051221	1559	26.779	55.948	15.4	2.3	85.79	86.92	24.67	218.4	14.03	313.69	20.25	A
69	20051222	629	26.745	55.984	14.3	3.1	66	45.38	0	2.96	16.71	267.79	16.71	A
70	20051222	2152	26.82	55.933	15.6	2	84.92	28.84	-14.1	343.7	13.57	75.23	6.28	A
71	20051223	1948	26.839	55.973	15.4	1.9	90	65	0	20	0	110	0	B
72	20051223	2023	26.846	56.008	14.7	1.9	82.78	72.05	16.53	205.06	6.36	296.98	16.77	A
73	20051224	118	26.862	55.976	15.2	2	82.73	306.34	5.32	261.11	1.4	170.89	8.89	A
74	20051225	1635	26.788	55.876	11.7	1.9	84.28	242.33	8.22	16.77	1.73	107.07	9.85	A
75	20051225	2045	26.792	55.862	15.5	1.9	85.02	247.3	8.68	21.71	2.58	112.14	9.66	A
76	20051227	128	26.824	55.817	12.7	2.5	82.56	264.44	29.15	34.07	14.48	131.19	25.66	B
77	20051227	354	26.799	55.846	14.4	2.9	83.91	252.08	12.63	25.88	4.52	116.95	13.22	A
78	20051227	2223	26.791	55.922	15.9	2.8	57.2	192.82	32.73	139.4	3.53	45.89	44.78	B
79	20051228	638	26.784	55.86	15	3	90	249.23	10	23.79	7.05	114.67	7.05	A
80	20051228	1143	26.834	55.962	16.1	2.7	66.87	255.12	6.57	210.97	11.73	116.48	20.62	A
81	20051229	121	26.81	55.963	14	1.7	79.53	165.48	-14.7	121.38	17.77	212.27	2.77	B
82	20051231	1806	26.83	55.958	16.3	2.3	83.72	169.65	-24.3	123.5	21.47	218.38	12.2	B
83	20051231	2229	26.813	55.988	15.6	2.9	85.54	80.47	33.74	209.11	19.67	309.39	26.53	A
84	20051231	2248	26.832	55.999	16.2	2.5	80.15	1.94	17.5	134.55	5.08	226.33	19.29	B
85	20060101	1631	26.824	55.992	16.6	3.3	82.04	255.25	-37.3	206.53	31.47	308.73	19.04	B
86	20060101	2238	26.824	55.996	15.2	3	78.07	0.2	13.57	133.63	0.93	223.93	17.97	B
87	20060104	53	26.814	55.92	12.7	2.1	54.07	27.72	37.45	331.96	3.83	237.43	49.74	A
88	20060104	950	26.806	55.893	14.9	2.9	81.99	58.62	4.11	13.54	2.77	283.12	8.56	A
89	20060105	2032	26.801	56.009	17.8	1.9	72	32.33	0	348.77	12.62	255.9	12.62	B
90	20060106	951	26.8	55.89	13	2.3	82.65	207.95	9.51	342.18	1.45	72.49	11.91	A
91	20060106	1443	26.783	55.899	13.3	2.1	90	212.33	18	345.9	12.62	78.77	12.62	B
92	20060106	2054	26.816	55.968	14.1	1.2	81.35	62.12	-5.04	17.72	9.66	287.28	2.58	B
93	20060107	209	26.846	56.003	12.7	2.8	52.24	79.82	26.57	29.86	10.55	289.83	43.08	B
94	20060107	313	26.825	55.97	14.3	1.7	90	15	0	330	0	60	0	B
95	20060108	1039	26.825	55.964	15	2.1	90	55	0	10	0	100	0	B
96	20060108	1239	26.833	55.9	14.3	2	72.77	93.65	10.31	47.95	5.08	316.17	19.29	B
97	20060108	2124	26.839	56	10.7	1.8	83.72	241.37	34.5	9.34	18.71	109.89	28.39	B
98	20060109	212	26.809	55.966	12.9	1.2	77.05	64.13	-7.63	20.5	14.48	289.51	3.84	B
99	20060110	10	26.741	55.933	13.8	1.9	78.6	106.42	-3.76	62.32	10.68	331.29	5.42	A
100	20060110	232	26.835	55.893	14.9	1.3	78.69	253.57	-16.6	209.59	19.68	300.81	3.4	B
101	20060110	340	26.748	55.931	14.2	1.7	80.15	102.65	1.75	57.91	5.72	327.09	8.18	B
102	20060110	1400	26.812	56.017	13	2	80.64	59.23	-25.4	13.8	24.5	108.71	10.64	B
103	20060110	1521	26.794	55.898	14.2	3.3	76.77	220.23	-15.1	176.81	19.97	267.18	1.03	B
104	20060110	1940	26.802	55.939	12.2	1.8	86.6	189.41	-19.7	143.31	16.27	236.66	11.31	B
105	20060111	38	26.823	55.885	12.5	2	66.12	30.44	23.49	340.89	1.63	249.83	32.95	B
106	20060111	1746	26.798	55.934	11.1	1.7	85.25	193.19	-19.5	147.4	17.05	240.55	10.15	B
107	20060111	2242	26.86	55.968	14.9	1.7	82.78	146.95	-16.5	102.02	16.77	193.94	6.36	B
108	20060112	2132	26.8	55.959	16.9	3.8	90	66	0	21	0	111	0	A
109	20060112	2142	26.797	55.964	16.3	1.8	90	56	0	11	0	101	0	B
110	20060112	2218	26.807	55.954	16.6	3.1	90	60	0	15	0	105	0	A
111	20060113	2108	26.834	55.979	15.4	2.8	60	234.44	0	193.55	20.7	95.34	20.7	A
112	20060113	2109	26.831	55.97	14	1.8	87.54	93.85	12.77	227.89	7.23	319.26	10.75	B
113	20060113	2123	26.836	55.973	15.3	1.8	75.29	251.72	31.01	19.7	9.95	116.02	32.13	B
114	20060114	302	26.808	55.946	15.4	2.3	85.25	193.19	-19.5	147.4	17.05	240.55	10.15	A
115	20060116	39	26.857	55.956	15.6	2	62.68	188.51	17.35	141.46	7.88	46.73	30.79	A
116	20060116	1354	26.795	55.917	13.4	3	82.56	209.15	-13.1	164.5	14.48	255.49	3.84	B
117	20060118	429	26.819	55.997	12.7	2	78.18	85.77	46.87	206.98	21.12	316.27	40.54	A
118	20060120	2050	26.817	55.976	14.9	2	86.47	15.11	3.54	330	0	240	5	A
119	20060120	2052	26.817	55.975	14.6	1.8	86.47	15.11	3.54	330	0	240	5	A
120	20060120	2100	26.809	55.969	14.5	2.2	79.45	52.8	44.01	175.74	20.7	282.76	37.76	B
121	20060120	2100	26.806	55.97	11.8	2	69.75	64.35	52.31	181.11	16.27	291.72	50.33	B
122	20060120	2101	26.813	55.971	15.3	2.3	90	42.59	41	169.63	27.64	275.55	27.64	B
123	20060121	1354	26.817	55.922	14.8	3.5	90	246.67	15	20.67	10.55	112.66	10.55	B
124	20060121	2233	26.85	55.96	12.5	1.5	87.42	303.35	-14.8	257.75	12.24	349.61	8.54	A
125	20060122	1634	26.853	55.959	14.7	1.6	76	209.2	0	165.06	9.85	73.34	9.85	B
126	20060122	1750	26.814	56.002	13.7	1.8	43.96	73.45	22.18	27.24	18.89	277.97	43.97	B
127	20060122	1935	26.854	55.985	14.5	2.3	60.82	258.15	30.19	205.85	1.97	114.15	40.93	B
128	20060122	2158	26.827	55.988	14	1.9	71.78	257.89	29.21	26.26	6.13	120.3	33.29	A
129	20060123	2355	26.839	55.976	14.6	2	87.56	203.88	-5.48	158.89	5.6	249.11	2.15	B
130	20060124	0	26.8	55.962	12.2	2.4	61.61	65.12	48.07	183.56	7.27	283.32	53.04	B

No	Date	Time	Lat	Lon	Depth	Mag	de1	Az1	R1	AzP	deP	AzT	deT	Q
131	20060124	48	26.802	55.957	12.4	1.9	72.61	207.63	42.19	330.32	14	73.12	41.64	B
132	20060124	1607	26.828	55.855	13.6	3.7	79.45	224.01	-10.7	180	15	270	0	A
133	20060125	48	26.827	55.862	11.3	1.3	70.32	230.7	-10	188.81	20.74	96.15	7.01	B
134	20060125	1232	26.822	55.988	14	3	83.65	70.32	44.65	193.91	24.56	302.49	34.89	A
135	20060125	1417	26.826	56.006	14.2	1.3	64.34	268.13	16.1	221.38	7.44	127.25	28.88	B
136	20060127	18	26.825	55.987	14.7	1.3	90	40	0	355	0	85	0	B
137	20060127	318	26.848	55.946	16.8	3.2	75.97	251.29	32.4	18.8	11.31	116.15	32.61	A
138	20060127	1825	26.808	55.972	11.9	2	85.79	14.92	24.67	146.4	14.03	241.69	20.25	B
139	20060127	2341	26.83	56.01	15	1.5	70.06	76.12	13.63	29.73	4.85	297.62	23.44	B
140	20060128	229	26.797	55.885	11.7	3.1	85.47	244.92	-2.12	200.07	4.7	109.93	1.71	A
141	20060128	231	26.805	55.864	13.2	1.3	75.07	236.87	33.15	3.97	11.03	101.46	33.76	A
142	20060129	1057	26.821	55.92	14.6	1.9	66.87	334.02	-6.57	292.66	20.62	198.18	11.73	A
143	20060129	2031	26.821	55.824	12	2.2	71.25	235.34	7.1	190.5	8.31	97.77	18.06	B
144	20060129	2204	26.816	55.826	12.4	2.8	77.34	228.5	-2.97	184.51	11	93.17	6.85	A
145	20060130	117	26.806	55.957	9.9	2.2	67.68	62.05	61.71	172.67	17.9	293.3	57.63	B
146	20060130	1522	26.829	55.978	14.7	1.7	76.14	211.97	1.99	167.55	8.37	75.89	11.14	A
147	20060130	1818	26.8	55.887	13	2.1	88.75	72.6	-5.87	27.52	5.03	117.81	3.26	A
148	20060131	2305	26.812	55.901	7	3	90	41.67	30	172.56	20.7	270.77	20.7	B
149	20060201	3	26.817	55.871	11.9	2.2	86.32	232.21	-17.6	186.45	15.02	279.08	9.69	A
150	20060201	1217	26.805	55.897	8	4.1	82.56	32.52	13.06	166.18	3.84	257.17	14.48	B
151	20060201	1803	26.847	56.018	12.5	1.3	48.16	50.73	10.97	9.12	21.8	262.92	34.89	A
152	20060201	1805	26.843	56.013	12	2.5	81.11	251.82	15.72	24.89	4.59	116.33	17.37	A
153	20060202	19	26.851	55.836	10	1.8	82.56	209.15	-13.1	164.5	14.48	255.49	3.84	B
154	20060203	647	26.821	55.873	10.1	2.7	76.43	30.77	6.46	345.63	5.08	254.35	14.08	B
155	20060204	2222	26.795	55.936	10.5	1.5	54.6	159.43	29.84	107.6	7.05	10.7	44.14	B
156	20060206	2121	26.833	55.982	14.1	1.7	80.15	65.84	28.48	195.32	12.2	291.63	26.95	B
157	20060206	2317	26.802	55.923	11.3	1.1	90	64	0	19	0	109	0	B
158	20060209	137	26.847	55.985	12.5	2.1	82	69.71	8.98	204.01	0.62	294.14	11.98	B
159	20060209	239	26.85	55.988	12.5	2.8	75.52	257.43	26.57	27.06	7.44	121.19	28.88	B
160	20060209	1144	26.847	55.851	11.3	3.3	80.8	220.41	3.94	175.4	3.73	84.79	9.27	A
161	20060209	2325	26.82	55.868	11.3	2.3	82.59	227.56	-6.73	183.05	9.99	92.95	0.52	B
162	20060210	13	26.829	55.983	15.4	1.7	87.54	44.24	17.84	177.49	10.72	270.25	14.29	B
163	20060210	58	26.848	55.991	13.2	2.1	65.92	35.39	12.59	349.64	8.5	255.56	25.42	B
164	20060211	2254	26.834	55.975	14.5	1.8	57.07	349.7	20.14	302.15	10.37	204.49	36.07	A
165	20060212	54	26.814	56.01	14.7	1.3	78.97	90.63	16.79	223.35	3.74	314.69	19.62	B
166	20060213	1108	26.834	55.955	14.6	2.1	63.86	349.46	20.89	300.99	4.89	207.86	32.54	A
167	20060215	829	26.8	55.981	16.9	3.1	84.52	64.38	17.17	197.41	8.06	289.74	15.98	B
168	20060215	1040	26.812	56.006	14.2	1.9	61.61	249.47	48.07	7.91	7.27	107.67	53.04	B
169	20060216	905	26.846	55.994	12.8	3	52.84	268.67	16.01	223.6	15.76	121.93	35.63	A
170	20060216	1333	26.839	55.997	15.2	1.8	75.29	252.3	22.9	23.13	4.97	115.61	26.46	A
171	20060216	2316	26.807	55.991	14.1	1.4	80.96	79.09	24.48	209.94	10.27	304.48	23.61	B
172	20060217	754	26.835	56.005	14.4	2.1	48.28	350.25	5.38	311.16	24.9	204.74	31.33	A
173	20060217	2245	26.824	56.01	14.2	1.2	87.85	79.56	-5.6	34.55	5.48	124.78	2.44	A
174	20060218	2033	26.813	55.885	12.3	3.1	82.56	209.15	-13.1	164.5	14.48	255.49	3.84	B
175	20060219	219	26.818	55.897	16	2.9	71.25	227.61	23.86	357.94	2.5	89.38	29.87	B
176	20060219	1928	26.857	55.97	15.3	3.1	90	232.5	22	5.34	15.36	99.66	15.36	B
177	20060220	110	26.886	55.929	13.2	2.6	72.91	351.03	5.73	306.31	8.06	213.99	15.98	B
178	20060220	112	26.889	55.929	14.6	2.6	75.52	172.17	3.97	127.52	7.44	35.8	12.95	B
179	20060220	116	26.89	55.928	13.3	3.5	75.52	172.17	3.97	127.52	7.44	35.8	12.95	B
180	20060220	129	26.88	55.926	12.7	2.1	82.36	173.73	-6.47	129.24	9.96	39.09	0.87	B
181	20060220	145	26.893	55.929	13.5	1.4	70.16	182.69	-2.54	139.87	15.64	46.42	12.16	A
182	20060221	2215	26.832	55.983	14.1	2.4	64.64	56.99	23.44	7.49	2.79	275.62	33.85	B
183	20060222	310	26.802	55.964	15.2	2.7	80.42	51.01	39.03	176.47	18.75	279.61	33.83	B

## References

- Ambraseys, N.N., Melville, C.P., 1982. A history of Persian Earthquakes, Cambridge Earth Science Series. Cambridge University Press, London.
- Bayer, R., Chéry, J., Tatar, M., Vernant, P., Abbasi, M., Masson, F., Nilforoushan, F., Doerflinger, E., Regard, V., Bellier, O., 2006. Active deformation in Zagros-Makran transition zone inferred from GPS measurements. *Geophysical Journal International* 165, 373–381.
- Berberian, M., 1995. Master blind thrust faults hidden under the Zagros folds: active basement tectonics and surface morphotectonics. *Tectonophysics* 241, 193–224.
- Engdahl, E.R., Jackson, J.A., Myers, S.C., Bergman, E.A., Priestley, K., 2006. Relocation and assessment of seismicity in the Iran Region. *Geophysical Journal International* 167, 761–778.
- Falcon, N.L., 1974. Southern Iran: Zagros mountains. In: Spencer, A. (Ed.), *Mesozoic-Cenozoic Orogenic Belts*, vol. 4. Spec. Publ. Geol. Soc., London, pp. 199–211.
- Haghypour, A., Aghanabati, A., 1996. Qeshm Geological and Mineral Research Studies. Qeshm Free Area. Sakoo Consulting Engineers, p. 522.
- Haghypour, A., Aghanabati, A., 2005. Geological Map of the Qeshm Area. Qeshm Free Area.
- Hatzfeld, D., Tatar, M., Priestley, K., Ghafory Ashtiani, M., 2003. Seismological constraints on the crustal structure beneath the Zagros Mountain belt (Iran). *Geophysical Journal International* 155, 1–8.
- Hessami, K., Koyi, H., Talbot, C., 2001. The significance of the strike-slip faulting in the basement of the Zagros fold and thrust belt. *Journal of Petroleum Geology* 24, 5–28.
- Hessami, K., Nilforoushan, F., Talbot, C.J., 2006. Active deformation within the Zagros Mountains deduced from GPS measurements. *Journal of the Geological Society*, London 163, 143–148.
- Jackson, J., Fitch, T., 1981. Basement faulting and the focal depths of the larger earthquakes in the Zagros mountains (Iran). *Geophysical Journal of the Royal Astronomical Society* 64, 561–586.
- Jackson, J., McKenzie, D.P., 1984. Active tectonics of Alpine-Himalayan belt between western Turkey and Pakistan. *Geophysical Journal of the Royal Astronomical Society* 77, 185–264.
- Kissling, E., 1988. Geotomography with local earthquake data. *Reviews of Geophysics* 26, 659–698.
- Lienert, B.R., Berg, E., Frazer, L.N., 1986. Hypocenter: An earthquake location method using centered, scaled, and adaptively least squares. *Bulletin of Seismological Society America* 76, 771–783.
- Nissen, E., Ghorashi, M., Jackson, J., Parsons, B., Talebian, M., 2007. The 2005 Qeshm Island earthquake (Iran)—a link between buried reverse faulting and surface folding in the Zagros Simply Folded Belt? *Geophysical Journal International* 171, 326–338.
- Nissen, E., Yaminifard, F., Tatar, M., Gholamzadeh, A., Bergman, E., Elliott, J.R., Jackson, J.A., Parsons, B., 2010. The vertical separation of mainshock rupture and microseismicity at Qeshm Island in the Zagros fold-and-thrust belt, Iran. *Earth and Planetary Science Letters* 296, 181–194.
- Ni, J., Barazangi, M., 1986. Seismotectonics of the Zagros continental collision zone and a comparison with the Himalayas. *Journal of Geophysical Research* 91, 8205–8218.

- Price, N.J., Cosgrove, J.W., 1990. Analysis of Geological Structures. Cambridge University Press, p. 502.
- Stöcklin, J., 1974. Possible ancient continental margins in Iran. In: Burk, C., Drake, C. (Eds.), *Geology of Continental Margins*. Springer-Verlag, New York, pp. 873–877.
- Stoneley, R., 1981. The geology of the Kuh-e Dalneshin area of southern Iran, and its bearing on the evolution of southern Tethys. *Journal Geological Society of London* 138, 509–526.
- Talebian, M., Jackson, J., 2004. A reappraisal of earthquake focal mechanisms and active shortening in the Zagros mountains of Iran. *Geophysical Journal Internat* 156, 506–526.
- Tatar, M., Hatzfeld, D., Martinod, J., Walsperdorf, A., Ghafory-Ashtiani, M., Chéry, J., 2002. The present-day deformation of the central Zagros from GPS measurements. *Geophysical Research Letter* 29, 1927–1930.
- Tatar, M., Hatzfeld, D., Ghafory-Ashtiani, M., 2004. Tectonics of the Central Zagros (Iran) deduced from microearthquake seismicity. *Geophysical Journal International* 156, 255–266.
- Vernant, P., Nilforoushan, F., Hatzfeld, D., Abbasi, M.R., Vigny, C., Masson, F., Nankali, H., Martinod, J., Ashtiany, A., Bayer, R., Tavakoli, F., Chéry, J., 2004. Present day crustal deformation and plate kinematics in the middle east constrained by GPS measurements in Iran and Northern Oman. *Geophysical Journal Internat* 157, 381–398.
- Waldhauser, F., Ellsworth, W.L., 2000. A double difference earthquake location algorithm: Method and application to the northern Hayward fault. *California, Bulletin Seismological Society of America* 90, 1353–1368.
- Walker, R.T., Bergman, E.A., Szeliga, W., Fielding, E.J., 2011. Insights into the 1968–1997 Dasht-e-Bayaz and Zirkuh earthquake sequences, eastern Iran, from calibrated relocations, InSAR and high-resolution satellite imagery. *Geophysical Journal International* 187, 1577–1603.
- Yaminifard, F., Hatzfeld, D., Tatar, M., Mokhtari, M., 2006. Microseismicity at the intersection between the Kazerun fault and the Main Recent Fault (Zagros-Iran). *Geophysical Journal International* 166, 186–196.
- Yaminifard, F., Hatzfeld, D., Farahbod, A.M., Paul, A., Mokhtari, M., 2007. The diffuse transition between the Zagros continental collision and the Makran oceanic subduction (Iran): Microearthquake seismicity and crustal structure. *Geophysical Journal International* 170, 182–194.